Detection of Polyps via Shape and Appearance Modeling

Paulo R. S. Mendonça,[1] Rahul Bhotika,[1] Fei Zhao,[1]
John Melonakos,[2] and Saad Sirohey[3]

[1]GE Global Research, One Research Circle, Niskayuna, NY 12309, USA
[2]School of ECE, Georgia Institute of Technology, Atlanta, GA 30332, USA
[3]GE Healthcare, Waukesha, WI 53188, USA

Abstract. This paper describes a CAD system for the detection of colorectal polyps in CT. It is based on stochastic shape and appearance modeling of structures of the colon and rectum, in contrast to the data-driven approaches more commonly found in the literature it derives predictive stochastic models for the features used for classification. The method makes extensive use of medical domain knowledge in the design of the models and in the setting of their parameters. The proposed approach was successfully tested on challenging datasets acquired under a protocol with little colonic preparation; such protocol reduces patient discomfort and potentially improves compliance.

1 Introduction

Early detection of polyps has been associated with reduction in the incidence of colorectal cancer [1], the fourth leading cause of cancer death worldwide [2], and optical colonoscopy has been shown to be an effective tool for polyp detection [3]. However, optical colonoscopy is an invasive procedure, and discomfort to the patient, in particular due to pre-examination colonic cleansing, has a negative impact on compliance [4].

The less invasive alternative of virtual colonoscopy has been shown to produce results at least as good as those of optical colonoscopy [5], even under protocols more amenable to the patient. However, this creates problems for radiologists, because such protocols leave the colon partially filled with fluid or stool.

The past decade has seen steady progress in the use of CAD algorithms for CT, such as the work of Yoshida *et al* [6], and Vos *et al* [7], which pioneered the use of curvature as a distinguishing feature segregating polyps from other colorectal structures. More recently, modeling through spherical harmonics [8], surface-normal overlap [9] and other curvature-based methods have been developed [10]. Finally, there has been a recent change in focus from CT exams in which the patient undergoes full colonic cleansing to less rigorous protocols [11]. The work described in this paper is in line with that important clinical trend.

2 Modeling of Colonic Structures

This section describes the extension of the Bayesian approach of [12] from the analysis of pulmonary to colonic structures. Let $\{\mathcal{M}_i, i = 1, ..., N\}$ be a set of models. Each $\mathcal{M}_i$ has parameters $\mathbf{m}_i$ in the domain $\mathbf{M}_i$. Given a choice of $\mathcal{M}_i$, $\mathcal{D}$ is assumed to be a set

$\mathcal{D} = \{\mathcal{D}_j, j = 1, ..., M\}$ of *independent* datum $\mathcal{D}_j$ associated with voxel $\mathbf{x}$. Using Bayes' law and marginalizing over the model parameters, we have

$$P(\mathcal{M}_i|\mathcal{D}, \mathbf{x}) = M! \times \frac{P(\mathcal{M}_i|\mathbf{x})}{p(\mathcal{D}|\mathbf{x})} \prod_{j=1}^{M} \int_{\mathbf{M}_i} p(\mathcal{D}_j|\mathbf{m}_i, \mathcal{M}_i, \mathbf{x}) p(\mathbf{m}_i|\mathcal{M}_i, \mathbf{x})\, d\mathbf{m}_i. \quad (1)$$

Following the majority of the works mentioned in section 1, we adopt the use of curvature as the feature for discriminating between polyps and the other colorectal structures, i.e., $\mathcal{D}_j = \boldsymbol{\kappa}(\mathbf{x}_j)$ for $\mathbf{x}_j \in B(\mathbf{x})$, where $B(\mathbf{x})$ is a neighborhood of $\mathbf{x}$. Once $p(\mathcal{D}_j|\mathbf{m}_i, \mathcal{M}_i, \mathbf{x})$ and $p(\mathbf{m}_i|\mathcal{M}_i, \mathbf{x})$ are available, Laplace's method [13] is used to compute the integral in (1), and label voxels in the image according to the value of $P(\mathcal{M}_i|\mathcal{D}, \mathbf{x})$.

2.1 Modeling the Likelihood Term

Colorectal structures relevant to the task of detecting polyps include sessile and pedunculated polyps, haustral folds, and the *haustra* or colon wall, each corresponding to a particular $\mathcal{M}_i$ in (1). Our approach to modeling $p(\mathcal{D}_j|\mathbf{m}_i, \mathcal{M}_i, \mathbf{x})$ for these structures is to first model their shape and/or appearance through simple analytical models, and then use an appropriate sampling procedure to sample from the analytical models and map the sampled points on the model to curvature values using either classical differential geometry or the geometry of Gaussian random fields [14].

2.2 Modeling the Prior

In this work, the modeling of the prior $p(\mathbf{m}_i|\mathcal{M}_i, \mathbf{x})$ in (1) relies heavily on the use of *domain knowledge* of the anatomy and pathology of colon. However, currently available clinical data is not enough to fully describe the probability density $p(\mathbf{m}_i|\mathcal{M}_i, \mathbf{x})$. One valuable technique to set up least-informative priors given the available constraints is the *maximum entropy principle* [15], which prescribes for $p(\mathbf{m}_i|\mathcal{M}_i, \mathbf{x})$ the probability density that maximizes $S = -\int p(x) \log p(x)\, dx$ given integral constraints in the form $E[f_k(x)] = c_k$, where E is the expectation functional. Clinical knowledge is incorporated in the functions f_k and the parameters c_k, mathematically encoding information such as expected values for polyp diameter [16] and width of colonic folds [17].

2.3 Geometric Models

Polyps and folds are modeled exclusively through geometry. The polyp model, $\mathcal{M}_1$, is chosen to be a solid ellipsoid given by

$$\mathcal{M}_1 : (\rho, \theta, \phi) \mapsto \mathbf{x} = \rho \begin{bmatrix} a\cos\theta\cos\phi & c\sin\theta\cos\phi & c\sin\phi \end{bmatrix}^{\mathrm{T}}, \quad (2)$$

where $\rho \in \Pi = [0, 1]$, $\theta \in \Theta = [0, 2\pi)$, and $\phi \in \Phi = [-\pi/2, \pi/2]$. The parameters of the model are $\mathbf{m}_1 = (a, c)$, with $a \leq c$. Each choice of $\rho \in \Pi$ defines a different surface at which principal curvatures can be computed, yielding

$$\rho = (a/c^2)\sqrt{\kappa_2/\kappa_1^3} \text{ and } \sin^2\phi = (c^2(\kappa_1/\kappa_2) - a^2)/(c^2 - a^2). \quad (3)$$

The maximum entropy prior on a non-negative random variable with finite mean is the exponential distribution. Under the constraint that $a \leq c$, we obtain the prior $p(\mathbf{m}_1|\mathcal{M}_1, \mathbf{x})$ given by (with $\mathbb{I}_X(x) = 1$ if $x \in X$ and 0 otherwise)

$$p(\mathbf{m}_1|\mathcal{M}_1, \mathbf{x}) = (8/5)\lambda^5 a^2 c e^{-\lambda(a+c)} \mathbb{I}_{\mathbf{M}_1}(\mathbf{m}_1), \tag{4}$$

where $2/\lambda$ is the expected diameter of a polyp in a given patient cohort.

A distribution over $\mathbf{x}$ can be obtained by sampling from $\mathcal{M}_1$ according to a Poisson point process, and through a succession of transformations of random variables, $\mathbf{x}$ is mapped to (ρ, θ, ϕ) according to (2) and (ρ, θ, ϕ) is mapped to $\boldsymbol{\kappa}$ according to (3). Finally, using a Laplace-type approximation [13] to solve the integral in (1), we have

$$p(\boldsymbol{\kappa}|\mathcal{M}_1, \mathbf{x}) \approx \frac{1536\lambda\kappa_2 f_{\boldsymbol{\kappa}}(f_{\boldsymbol{\kappa}}(g(\boldsymbol{\kappa}) + 3))}{11\,(3\kappa_1 + 5\kappa_2)^4} e^{-g(\boldsymbol{\kappa})} \mathbb{I}_{[0,\kappa_2]}(\kappa_1), \tag{5}$$

where $g(\boldsymbol{\kappa}) = \lambda(3\kappa_1 + 5\kappa_2)/[\kappa_2(3\kappa_1 + \kappa_2)]$ and $f_{\boldsymbol{\kappa}}(u) = g(\boldsymbol{\kappa})u + 6$.

Due to space limitations we cannot describe the derivation of the haustral fold model even at the scarce level of detail of (5), but the procedure is similar.

2.4 Appearance and Mixed Models

It is important to observe that the polyp and fold models are invariant to any monotonically increasing image intensity transformation of the CT data. This is due to the fact that those transformations preserve the geometry of isosurfaces in the volume, affecting only the isovalue associated with a given isosurface.

In contrast, the proposed *haustra* and *outlier* models are appearance-dependent, and are based on recent results in the theory of Gaussian random fields [14]. The modeling of the haustra has been introduced elsewhere [18], where it is shown how appearance and shape can be combined to derive an estimate for the probability distribution of curvatures on the colon wall. Assuming a simple spherical model of radius R for the colon wall, the probability distribution of the haustral curvatures is given by

$$p(\boldsymbol{\kappa}|\mathcal{M}_3, \mathbf{x}) = \frac{\kappa_2 - \kappa_1}{8\sqrt{2\pi}\alpha^3} \exp\left[-\frac{(5{\kappa_1}^2 - 6\kappa_2\kappa_1 + 5{\kappa_2}^2)R^2 + 4(\kappa_1 + \kappa_2)R + 4}{32R^2\alpha^2}\right], \tag{6}$$

with $\alpha = \sigma_\eta/(2\sigma^2 C)$, where σ_η is the amplitude of the image noise, σ is the scale parameter of a combined point-spread function and image-smoothing kernels, and C is the magnitude of the air-tissue gradient at the colon wall.

The outlier model is simply a particular case of the result in [14], which establishes the probability distribution of the curvature of isosurfaces at arbitrary points in an isotropically correlated Gaussian random field. The result depends only on the dimension n of the Euclidean vector space on which the random field is embedded, and the second and fourth derivatives of its autocorrelation function $R(\boldsymbol{\tau})$ at $\boldsymbol{\tau} = \mathbf{0} \in \mathbb{R}^n$. In our case, $n = 3$, and assuming that a good approximation for the image autocorrelation function can be derived from the CT system point-spread function and smoothing kernel, the resulting probability distribution is (with σ as in (6))

$$p(\boldsymbol{\kappa}|\mathcal{M}_4, \mathbf{x}) = \frac{256\sigma^3(\kappa_2 - \kappa_1)}{\pi(4 + 3\sigma^2\kappa_2^2 - 2\sigma^2\kappa_2\kappa_1 + 3\sigma^2\kappa_1^2)^3} \mathbb{I}_{(-\infty,\kappa_2]}(\kappa_1). \tag{7}$$

One issue not considered so far is what effect the immersion in colonic fluid should have over $p(\mathcal{D}_j|\mathbf{m}_i, \mathcal{M}_i, \mathbf{x})$. The key observation is that for polyps, folds, or haustra immersed in fluid, the general shape of the structure is preserved, but the gradient directions in the image are inverted. As a consequence, curvature values are also inverted, since the gradient is normal to the local isosurface, yielding $p'(\boldsymbol{\kappa}|\mathcal{M}_i, \mathbf{x}) = p'(\kappa_1, \kappa_2|\mathcal{M}_i, \mathbf{x}) = p(-\kappa_2, -\kappa_1|\mathcal{M}_i, \mathbf{x})$, where p' is the probability density of curvatures given $\mathcal{M}_i$ at fluid-immersed voxels $\mathbf{x}$.

3 Bayesian Classifier

Two pieces of information are still missing for the computation of (1). The first is $P(\mathcal{M}_i|\mathbf{x})$, which can be readily obtained from anatomical and epidemiological information on a screening patient cohort, in particular polyp prevalence and size distribution [16, 17]. Once such an estimate is available, $P(\mathcal{M}_i|\mathbf{x})$ can be computed as a relative volume ratio. For example, $P(\mathcal{M}_1|\mathbf{x})$ is given by the ratio of the expected volume of polyps per patient and the expected volume of all colonic structures.

The second missing component of (1) is more subtle. The distributions $p(\boldsymbol{\kappa}|\mathcal{M}_i, \mathbf{x})$ were derived under the assumptions that the voxel $\mathbf{x}$ has been sampled from model $\mathcal{M}_i$. However, the datum $\mathcal{D}_j$ in $p(\mathcal{D}_j|\mathcal{M}_i, \mathbf{x})$ has been extracted from a voxel $\mathbf{x}_j \neq \mathbf{x}$. To account for this we first, assume that the voxels of model $\mathcal{M}_i$ are located in a spherical region $\mathcal{R}$ of radius S, where S can be estimated from $p(\mathbf{m}_i|\mathcal{M}_i, \mathbf{x})$. If $\mathbf{x}$ is sampled from $\mathcal{R}$ according to a Poisson point process, and a voxel $\mathbf{x}_j$ is subsequently sampled among the set of all voxels at a distance d from $\mathbf{x}$, also according to a Poisson point process, the probability $w_{d,S}$ that $\mathbf{x}_j$ belongs to $\mathcal{R}$ can be computed as $w_{d,S} = (d - 2S)^2(d + 4S)/16S^3\mathbb{I}_{S \geq d/2}(S)$. Based on this simple model, we derive

$$p(\mathcal{D}_j|\mathcal{M}_i, \mathbf{x}) = w_{\|\mathbf{x}_j - \mathbf{x}\|,S}\, p(\boldsymbol{\kappa}|\mathcal{M}_i, \mathbf{x}) + (1 - w_{\|\mathbf{x}_j - \mathbf{x}\|,S}) p(\boldsymbol{\kappa}|\mathcal{M}_4, \mathbf{x}). \tag{8}$$

The probability (1) is computed for each voxel on the colon surface and each choice of model $\mathcal{M}_i$. Voxels for which the log-likelihood ratio $\log(P(\mathcal{M}_1|\mathbf{x})/\sum_{i \neq 1} P(\mathcal{M}_i|\mathbf{x}))$ is above a certain threshold are labeled as belonging to a polyp, and after running a connected components algorithm on the labeled data we obtain a set of candidate detections. Such detections are further thresholded on their average log-likelihood, and sweeping on this last threshold produces an fROC curve.

4 Experimental Results

Several studies have been published to measure efficacy of CT-based colon screening [19, 20] and CAD performance [11], but the only database publicly available is from WRAMC (http://imaging.nci.nih.gov[1]). Enlisted patients received an oral administration of 90 ml of sodium phosphate and 10 mg of bisacodyl, and followed a clear-liquid diet of 500 ml of barium for stool tagging and 120 ml of diatrizoate meglumine and diatrizoate sodium for fluid tagging. For details see [5]. The complete WRAMC database

[1] Courtesy of Dr. Richard Choi, Virtual Colonoscopy Center, Walter Reed Army Medical Center.

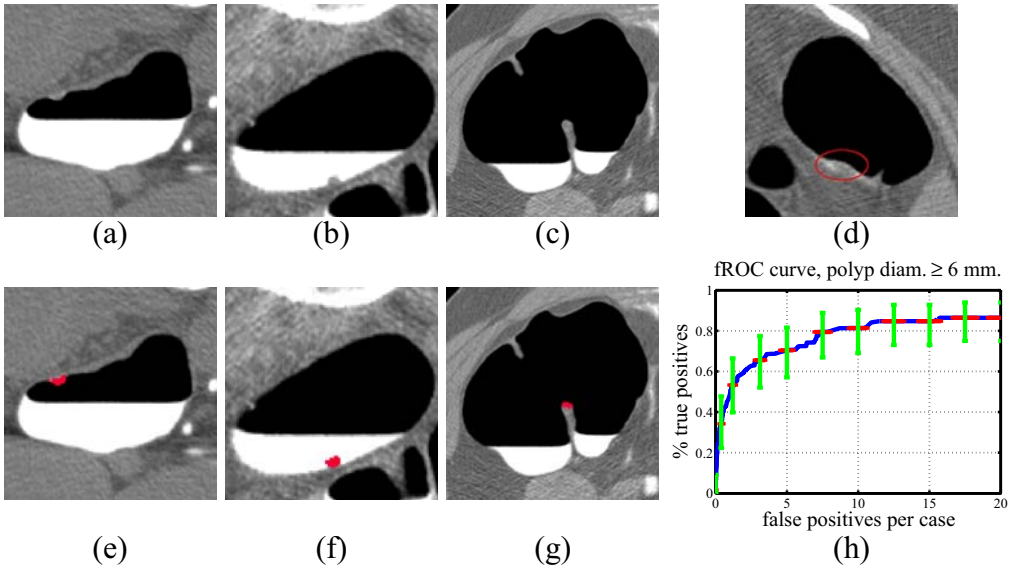

Fig. 1. Examples of correctly detected polyps in air (a) and fluid (b) regions, as shown in (e) and (f), respectively. The image in (c) shows a protruding tip on a fold incorrectly marked by the algorithm, as shown in (g). (d) depicts a flat sessile polyp missed by the algorithm. Figure (h) is the fROC curve for the dataset described in section 4.

consists of thousands of patients, but ground truth is provided only as the distance from each polyp to the rectum along the colon centerline. Therefore, we enlisted an expert who translated these coordinates into image locations for a subset of 46 patients. Each patient was scanned in prone and supine positions, giving 92 scans altogether, containing 59 polyps, both sessile and pedunculated, with diameter above 6 mm, the minimum lesion size for which follow-up is recommended under current protocols [20].

The algorithm performance is summarized in figure 1, which depicts detections for polyps immersed in air and in fluid, a false positive (FP) detection on the tip of a fold, and an undetected flat sessile polyp. At 10 FP/case, the algorithm reached a sensitivity of 83% for polyps with diameter equal to or above 6 mm. This result can be compared with those in [11], obtained with the full WRAMC dataset, and theferore the same imaging protocol. In Table 1 of that reference an fROC curve for a test set containing polyps with diameter of at least 6 mm is shown, depicting the sensitivity and FP rate *per patient*. If we conservatively assume that the corresponding FP *per case* in [11] is half of their FP rate per patient — which implies perfect reconciliation of independent detections on prone and supine volumes — they have achieved, at their chosen rate of 7.9 FP/patient (or 3.95 FP/case), a sensitivity of 61.3% (table 3). At that same FP rate we achieve 67.8% sensitivity, or, alternatively, at that same sensitivity we observe only 2.4 FP/case, a clearly superior performance.

5 Conclusions and Future Work

This paper presented an algorithm for detection of polyps depicted in CT images based on techniques of geometric probability. It follows a Bayesian framework, in which para-

metric models and statistical priors are derived from medical domain knowledge, rather than learned from data. It handles multiple protocols for patient preparation, in particular those that facilitate patient compliance. This is a key issue for the successful application of virtual colonoscopy in a large-scale screening program.

References

1. Winawer, S., Fletcher, R., Rex, D., Bond, J., Burt, R., Ferrucci, J., Ganiats, T., Levin, T., Woolf, S., Johnson, D., Kirk, L., Litin, S., Simmang, C.: Colorectal cancer screening and surveillance: Clinical guidelines and rationale — update based on new evidence. Gastroenterology **124**(2) (2003) 544–560
2. Ferlay, J., Bray, F., Pisani, P., Parkin., D.M.: GLOBOCAN 2002: Cancer incidence, mortality and prevalence worldwide. Technical report, IARC CancerBase No. 5. version 2.0, IARCPress, Lyon, France (2004) http://www-dep.iarc.fr/.
3. Smith, R.A., Cokkinides, V., Eyre, H.J.: American cancer society guidelines for the early detection of cancer, 2006. CA Cancer J. Clin. **56**(1) (2006) 11–25
4. Harewood, G.C., Wiersema, M.J., III, L.J.M.: A prospective, controlled assessment of factors influencing acceptance of screening colonoscopy. The American Journal of Gastroenterology **97**(12) (2002) 3186–3194
5. Pickhardt, P.: Target lesion: The radiologist's perspective. In: Sixth International Symposium on Virtual Colonoscopy, Boston, MA (2005) 60–62
6. Yoshida, H., Näppi, J.: Three-dimensional computer-aided diagnosis scheme for detection of colonic polyps. TMI **20**(12) (2001) 1261–1274
7. Vos, F.M., Serlie, I.W.O., van Gelder, R.E., Post, F.H., Truyen, R., Gerritsen, F.A., Stoker, J., Vossepoel, A.M.: A new visualization method for virtual colonoscopy. In: MICCAI. (2001) 645–654
8. Kiss, G., Van Cleynenbreugel, J., Drisis, S., Bielen, D., Marchal, G., Suetens, P.: Computer aided detection for low-dose CT colonography. In: MICCAI. (2005) 859–867
9. Paik, D.S., Beaulieu, C.F., Rubin, G.D., Acar, B., Jeffrey, Jr., R.B., Yee, J., Dey, J., Napel, S.: Surface normal overlap: A computer-aided detection algorithm with application to colonic polyps and lung nodules in helical CT. TMI **23**(6) (2004) 661–675
10. van Wijk, C., van Ravesteijn, V.F., Vos, F.M., Truyen, R., de Vries, A.H., Stoker, J., van Vliet, L.J.: Detection of protrusions in curved folded surfaces applied to automated polyp detection in CT colonography. In: MICCAI. (2006) 471–478
11. Summers, R.M., Yao, J., Pickhardt, P.J., Franaszeklow, M., Bitterlow, I., Brickmanlow, D., Krishnalow, V., Choi, J.R.: Computed tomographic virtual colonoscopy computer-aided polyp detection in a screening population. Gastroenterology **129** (2005) 1832–1844
12. Mendonça, P.R.S., Bhotika, R., Zhao, F., Miller, J.V.: Lung nodule detection via Bayesian voxel labeling. In: Int. Conf. on Information Proc. and Medical Imaging. (2007) 134–145
13. Kass, R.T., Raftery, A.E.: Bayes factors. J. Amer. Statist. Assoc. **90**(430) (1995) 773–795
14. Mendonça, P.R.S., Bhotika, R., Miller, J.V.: Probability distribution of curvatures of isosurfaces in Gaussian random fields. http://arxiv.org/pdf/math-ph/0702031 (2007)
15. Jaynes, E.T.: Probability Theory: The Logic of Science. Cambridge University Press (2003)
16. Pickhardt, P.J., Choi, J.R., Hwang, I., Butler, J.A., Puckett, M.L., Hildebrandt, H.A., Wong, R.K., Nugent, P.A., Mysliwiec, P.A., Schindler, W.R.: Computed tomographic virtual colonoscopy to screen for colorectal neoplasia in asymptomatic adults. N. Engl. J. Med. **349**(23) (2003) 2191–2200
17. Langer, P., Takacs, A.: Why are taeniae, haustra, and semilunar folds differentiated in the gastrointestinal tract of mammals, including man? J. Morph. **259**(3) (2004) 308–315

18. Melonakos, J., Mendonça, P.R.S., Bhotika, R., Sirohey, S.A.: A probabilistic model for haustral curvatures with applications to colon cad. In: MICCAI. (2007) 420–427
19. Johnson, C.D.: The national CT colonography trial: ACRIN protocol 6664 (2006)
20. Kim, D.H., Pickhardt, P.J., Taylor, A.J., Leung, W.K., Winter, T.C., Hinshaw, J.L., Gopal, D.V., Reichelderfer, M., Hsu, R.H., Pfau, P.R.: CT colonography versus colonoscopy for the detection of advanced neoplasia. N. Engl. J. Med. **357**(14) (2007) 1403–1412